

Article

Accuracy Assessment on Unmanned Aerial System Derived Digital Surface Models

Salvatore Manfreda ¹, Petr Dvorak ², Jana Mullerova ³, Sorin Herban ⁴, Pietro Vuono ⁵, José Juan Arranz Justel ⁶, Matthew Perks ⁷

¹ Dipartimento delle Culture Europee e del Mediterraneo: Architettura, Ambiente, Patrimoni Culturali (DiCEM), Università degli Studi della Basilicata, 75100 Matera, Italy; salvatore.manfreda@unibas.it

² Institute of Aerospace Engineering, Brno University of Technology, Technická 2, 61669 Brno, Czech Republic; dvorak.p@fme.vutbr.cz

³ Department GIS and Remote Sensing, Institute of Botany of the Czech Academy of Sciences, 252 43 Pruhonice, Czech Republic.; jana.mullerova@ibot.cas.cz

⁴ Politehnic University of Timisoara, Traian Lalescu 2^o, 300223 Timisoara, Romania; sorin.herban@upt.ro

⁵ Scuola di Ingegneria, Università degli Studi della Basilicata, 85100 Potenza, Italy; pietro.vuono@unibas.it

⁶ ETSI Topografía, Geodesia y Cartografía, Universidad Politécnica de Madrid; josejuan.arranz@upm.es

⁷ School of Geography, Politics and Sociology, Newcastle University, Newcastle upon Tyne NE1 7RU, UK; matthew.perks@newcastle.ac.uk

* Correspondence: salvatore.manfreda@unibas.it; Tel.: +39-0971 205139

Abstract: Small unmanned aerial systems (UAS) represent a cost-effective strategy for topographic surveys. These low-cost drones can provide useful information for 3D reconstruction even if they are equipped with a low-quality navigation system. To ensure the production of high-quality topographic models, careful consideration of flight mode and proper distribution of ground control points is required. To this end a commercial drone has been adopted to monitor a small earthen dam using different combinations of flight configurations and adopting a variable number of ground control points (GCPs). Results highlighted that both choice and combination of flight plans can reduce the relative error of the 3D model up to a few meters without the need of including GCPs. The use of GCPs allows the quality of topographic survey to be greatly improved, reducing error to the order of a few centimeters. In particular, the combined use of images extracted from two flights, one with a camera mounted at nadir and the second with a 20° angle, proves extremely beneficial to increase the overall accuracy of the 3D model and especially of the vertical precision.

Keywords: Topographic surveys, UAS, DSM, GCPs, SfM, MVS.

1. Introduction

Unmanned aerial systems (UAS) are getting increasingly popular for many environmental applications, delivering frequent and very high-resolution digital surface/elevation models (DSM/DEMs) and orthoimagery [1-3]. High precision is crucial for many applications, especially for change detection studies [e.g. 4, 5]. Traditionally, DSMs are delivered using terrestrial or aerial surveys (laser scanning), which are often time-consuming, difficult to organize, and costly [6]. Structure from Motion (SfM) and multi-view stereo (MVS) algorithms allow creation of DSMs and orthomosaics without prior information on camera parameters such as focal length or radial distortion, and provide a flexible and low-cost alternative, enabling high temporal frequency and optimal timing of the mission [7, 8].

The accuracy of SfM-derived DSMs is highly variable, and the causes are still not fully understood (see the review by Smith and Vericat [9]). A number of factors may affect precision of UAS-derived orthoimagery and digital elevation data, such as flight parameters (e.g. elevation above ground level - AGL, flight speed, direction, orientation of the camera, camera's focal length, etc.), image quality, processing software, morphology of the studied area, and type of vehicle (fixed or

rotary wing). For instance, flight at low altitudes often requires short focal length lenses to be fitted to the camera in order to maintain sufficient coverage of the terrain. These lenses often introduce considerable geometric distortion into the imagery and thus overall accuracy is compromised.

It should be also stated that most available SfM software operates like a black-box with several default parameter settings. It has been shown that appropriate settings can reduce positioning error of SfM-MVS products [10], but processing workflow and accuracy assessment methodology need to be optimized and standardized [8, 11].

In this context, ground control points (GCPs) are a commonly used to increase the precision of products, even though their collection represents a laborious and time intensive part of UAS campaigns. The literature offers a wide spectra of choices for the number and spatial distribution of GCPs used to support SfM-MVS algorithms. A selection of the most recent publications dealing with the impact of GCPs configurations/number on DSM quality is reported in Table1. Such experiences taken individually do not provide a clear guidance for the identification of the appropriate number of GCPs, but they provide a valuable source of information for the definition of some preliminary guidelines.

In particular, we harmonized the information contained in the mentioned references extracting all available data in terms of DSM planar and vertical accuracy. These data are summarized in Figure 1 that describes the measured planar and vertical Root Mean Square Error (RMSE) as a function of the GCPs density. This allows to compare outcomes of different studies and better identify general tendencies. According the analyzed literature, DSM accuracy tends to increase with the number of GCPs adopted reaching rapidly an asymptotic behavior. Commonly for all the experiments, errors observed on the vertical precision are systematically higher compared to the horizontal one. It can be noticed that planar errors decrease more rapidly with the increase of GCPs in comparison to vertical errors. In this graph, the planar error tends to stabilize when the GSP density exceeds 5, while 10 GCPs/ha are needed to reach the same condition on vertical precision. This emphasizes the need to find new strategies to improve DSM accuracy especially in elevation estimates.

Reference	Area [ha]	Number of GCPs	AGL [m]	RMSE _{x,y} [cm]	RMSE _z [cm]	RMSE Total [cm]
Rock et al. [12]	N/A	1042	50-550	N/A	5.5	N/A
Tahar [13]	150	8-9	N/A	50.0	78.0	N/A
Mancini et al. [14]	2.75	18	40	0.8	10.0	N/A
Hugenholtz et al. [15]	4.5	28	200	18	29	N/A
Lucieer et al. [4]	0.75	39	N/A	7.4	6.2	N/A
Cryderman et al. [16]	7.12	11	118	3.3	3.1	4.6
Gómez-Candón et al. [17]	1.0	11-45	30-100	N/A	N/A	0.29-0.12
Uysal et al. [18]	5.0	27	60	N/A	6.62	N/A
Kung et al. [19]	210.0	19	262	38	107	125
Agüera-Vega et al. [20]	17.64	4-15-20	120	7-4.5-1.7	33-5.8-4.7	N/A
Koci et al. [21]	41-45-72	6-7	100	N/A	30.9-68.7-95.9	N/A
James et al. [17]	7.5	4-27	100	4.9-	N/A	1.6
Oniga et al. [22]	1.0	3-40	28-35	4.5-8.9	6.6-4.0	7.4-7.9

Table 1. Precision of DSMs created using a variable number of GCPs, examples extracted from the literature.

The literature review offered useful indications about the optimization of the number of GCPs, but synergic effects of their number and spatial arrangement, as well as flight characteristics are still not fully understood [see 5, 17, 20]. Optimizing UAS campaigns would therefore make an important step towards the effectiveness and reliability of UAS-derived products.

In the present manuscript, we explore the impact of both UAS flight characteristics (e.g., altitude, camera tilt, and flight plan) and GCPs density on the accuracy of a 3D model of a small earthen dam. Analyses help understanding the procedure to increase the reliability of digital surface models (DSMs) that represent a critical information in environmental and hydrological science.

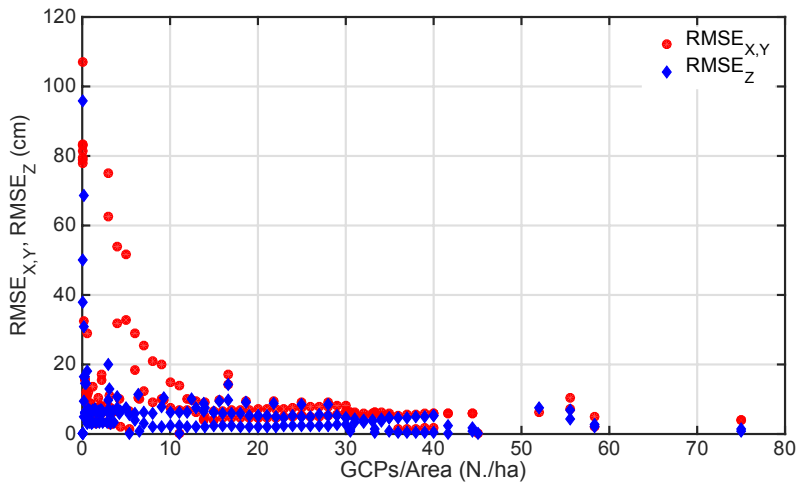


Figure 1. DSM accuracy in terms of planar and vertical RMSE as a function of the GCPs density (data extracted from the literature reported in Table 1).

2. Materials and Methods

2.1. Study area

The survey experiment was executed on an earthen dam next to the village Pișchia, 20 kilometers northwest from Timisoara (western Romania). The Pișchia dam, managed by National Water Administration, has a volume of approximately 500,000 m³, which is used to supply drinking water and for recreation activities (e.g., fishing). It has a trapezoidal cross section with side slope of 1:3 and a maximum elevation of about 10 m. The surrounding area is characterized by agricultural land with gentle slopes (Figure 2).

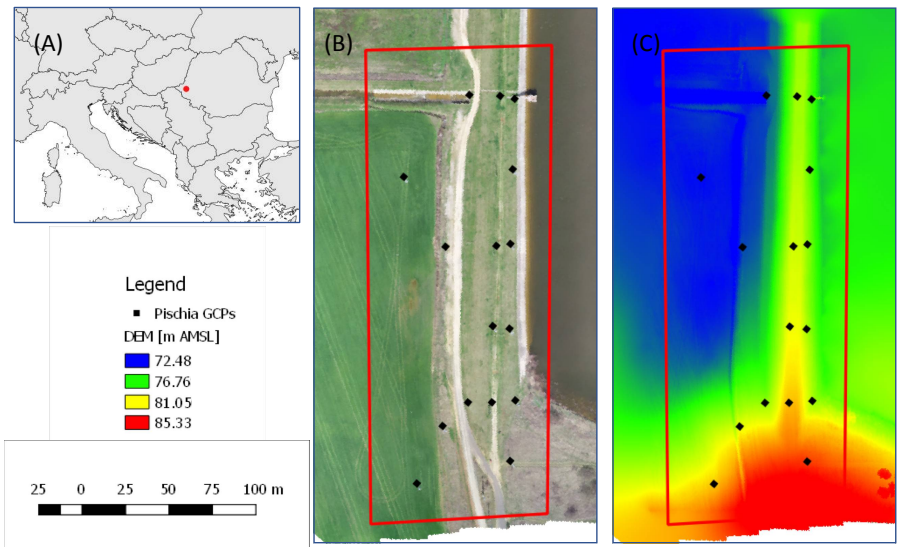


Figure 2. A) Position of the study area within Europe (45.927N, 21.335E). B) Description of the study area and distribution of the GCPs. C) UAS-derived DSM of the area.

2.2. Primary data collection

All flights were performed with DJI Phantom 4 Pro quadcopter, featuring a gimbaled 20 Mpix 1" sensor with mechanical shutter. Focal length of the lens was 24 mm (full-frame equivalent). The data were stored in 24 bit JPG format, pixel size was 2.41 um. Camera sensitivity was set at ISO100 for all images with aperture ranging from 4 to 5.6 and shutter times ranging between 1/120-1/500. All images were georeferenced with the on-board GPS. The WGS84 coordinates were stored in JPG EXIF.

Mission planning was executed in Pix4Dcapture that enabled control of the camera tilt. All six flights were performed between 10:00 and 12:50 UTC. Flight missions were planned using side overlap of 60%, and a front overlap of 80%.





Flighth	Flighth Plan	Level Above the Ground (m)	Camera Tilt (degree)	Avg GSD (cm/px)	Number of Images
N.1		60	0°	1.9	276
N.2		60	0°	1.9	268
N.3		60	70°	-	271
N.4		60	20°	2.0	273
N.5		60	0°	1.9	257
N.6		120	0°	3.3	85

Table 2. Characteristics of the different surveys carried out during the experiment.

In order to explore the impact of mission planning on the overall accuracy of UAS-derived DSM, different flight plans have been performed changing flight trajectories, camera tilt, and elevation of the flight. The variable characteristics of the six flights are summarized in Table 2, while other parameters such as camera settings and additional mission flight settings (e.g., overlap) are kept constant. Some examples of the images obtained by different configurations are shown in Figure 3, where an area from the central part of the dam is reproduced. From these images one can recognize the outlet tower and the spillway of the dam.

The survey was carried out on 4th April 2018 between 10:00 and 12:50 UTC. Flights were planned to cover an area of approximately 100 x 270 m (about 2.7 ha), an extent highlighted in Figure 2.B (see red line boundaries). In the same figure, we also report the UAS-derived Digital Surface Model (DSM) of the area.

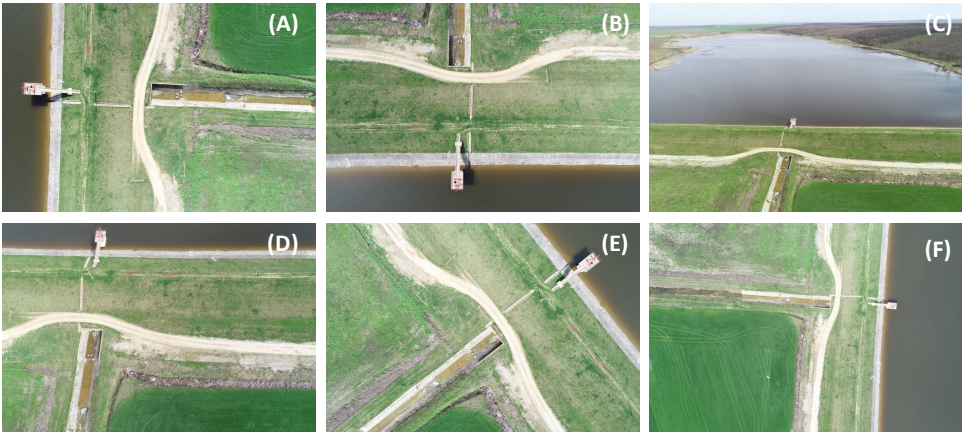


Figure 3. Images of the central part of the dam body acquired during flight N.1 (A), N.2 (B), N.3 (C), N.4 (D), N.5 (E), and N.6 (F).

For the aim of the present study, only a portion of the dam has been studied using about 16 GCPs distributed along the dam main structure and in the adjacent agricultural area. They have been placed along five longitudinal alignments trying to measure the full range of elevation changes. Maximum vertical variation of GCPs is about 10.6 m.

The GCP positions were determined using a Leica 1200 system of RTK GNSS rover and a precise Leica 1201 Total Station with a view to achieve a precision better than 3 mm for all GCPs. To determine a geodetic base, corrections were acquired from the Romanian Position Determination System (ROMPOS) network of GNSS permanent stations.

2.3. Data Processing

Images retrieved by each flight were processed using Agisoft PhotoScan ver. 1.4.3 to derive a 3D model of the area. The same workflow was repeated each time keeping constant the software settings, following sequence of commands: 1) Photo alignment with high accuracy; 2) Optimizing alignment; 3) Dense cloud building with high quality + aggressive depth filtering; 4) Mesh building using a sparse cloud; 5) Texture building with default blending mode; 6) Tiled model building; 7) DSM building using default settings; 8) Orthomosaic generation.

In a preliminary phase, we focused on the use of the geotagged images alone excluding the use of GCPs. Measured GCPs have been adopted as check points only to validate the results. Elaboration carried out without GCPs allowed us to better understand the role of flight mode and combination of different flights on the resulting DSM. This was made possible by exploring accuracies of DSMs obtained using imagery extracted from a single flight and from the combinations of two flights. Resulting combinations displayed a wide variability in the precision of planar coordinates and elevation. This preliminary analysis allowed identifying the best performing flight configuration and also the benefit due to the use of combined flights.

To increase the quality in the 3D model, GCPs can be included in the elaboration for georectification. Number and distribution of GCPs per unit area are not univocally identified in literature as highlighted in the introduction [see e.g., 23]. In fact, the number of GCPs necessary for the survey is influenced by the extent of the study area and its morphology, camera deployed, drone GPS precision, and the type of the survey.

According to the analysis carried out without GCPs, two groups of images extracted from a single flight and from two flight missions were selected to explore the role played by the GCPs density and distribution. A random number of GCPs ranging from 1 up to 9 was used in this second phase, while the remaining GCPs were employed as check points. This second analysis was extremely useful to understand the mutual benefit of combination of flights and a well-designed GCP distribution. Proper use of these two settings emphasize the potential of SfM-MVS algorithms in providing good quality DSMs. The comparison between single and multiple flights combined with the use of GCPs was stimulated by the need to better understand the benefits of combining multiple flights.

3. Accuracy assessment of the 3D models

3.1. Impact of mission planning on DSM

Results of the quality assessment based on individual flights with different settings (for details see Table 2) and their combinations are summarized in Table 3, where we reported the Root Mean Square Error (RMSE) estimated between the 3D model derived by the SfM-MVS algorithms of PhotoScan and the 16 check points distributed in the area. The table provides four groups of information in the following order, starting from the upper part: the planar error of the topographic surface, the absolute elevation, the relative elevation defined as elevation reduced by the minimum value observed among the considered validation points, and the total error obtained as the sum of planar and vertical error. Columns and rows identify the combination of flights adopted for the analysis including single flight configurations reported on the diagonal of each table.

These preliminary results summarize the impact of flight configuration on DSM accuracy. It can be observed that the relative error in planar coordinate is significantly lower in respect to the vertical absolute error. In fact, the SfM-MVS estimated elevation is affected by an error of one or two orders of magnitude larger than planar georeferencing. Such a systematic error becomes less critical when taking into consideration the relative elevation of the surface. Another result is represented by the

low quality of the 3D models derived with images taken with a camera tilted of 70°. Such a camera configuration produces images with limited amount of information that deteriorates the result in all combinations, especially for planar coordinates. This survey becomes beneficial only in reducing the error of the absolute elevation of the DSM, but its value is limited in terms of relative elevation (see third panel of Table 3).

Planar Coordinates - RMSE _{XY} (m)						
Flight	N. 1	N.2	N. 3	N. 4	N. 5	N. 6
N. 1	4.47					
N.2	2.39	2.03				
N. 3	136.05	1497.25	X			
N. 4	1.64	3.08	3835.20	7.75		
N. 5	2.09	1.95	15042.56	8.05	7.15	
N. 6	3.06	3.35	1750.11	8.63	6.94	19.70
Elevation - RMSE _z (m)						
Flight	N. 1	N.2	N. 3	N. 4	N. 5	N. 6
N. 1	82.90					
N.2	81.18	78.72				
N. 3	80.32	56.94	X			
N. 4	79.21	76.94	15.51	75.02		
N. 5	77.90	77.86	7.70	73.35	71.86	
N. 6	78.79	75.48	20.25	72.85	70.27	59.75
Relative Elevation - RMSE _z (m)						
Flight	N. 1	N.2	N. 3	N. 4	N. 5	N. 6
N. 1	1.06					
N.2	0.39	0.37				
N. 3	3.74	19.55	X			
N. 4	0.55	0.42	5.88	0.11		
N. 5	0.39	0.25	8.00	0.47	0.26	
N. 6	0.22	0.94	13.85	0.80	0.40	3.44
Planar and vertical - RMSE (m)						
Flight	N. 1	N.2	N. 3	N. 4	N. 5	N. 6
N. 1	4.59					
N.2	2.42	2.06				
N. 3	136.10	1497.38	X			
N. 4	1.73	3.11	3835.20	7.75		
N. 5	2.13	1.97	15042.56	8.06	7.15	
N. 6	3.07	3.48	1750.16	8.67	6.95	20.00

Performances

High

Medium

Low

Table 3. RMSE estimated on 16 GCPs for planar coordinates, absolute elevation, relative elevation defined as elevation reduced by the minimum value observed among the considered validation points, and the sum of the planar and vertical error obtained using different images taken from different flight combinations (for description see Table 2). The values written in bold represent the best performing configuration for each specific sub-group.

The best results in terms of planar coordinates were obtained combining the flights N. 1 and N. 4, while the best performances in terms of relative elevation was obtained with the flight N. 4. It can be observed that all combinations including flight N. 4 provided an improvement in the accuracy of the relative elevation. Considering the sum of the planar and vertical errors (considering the relative elevation), the best performing set of images was obtained by the combination of flight N. 1 and N. 4. Among the tests based on a single flight, the results obtained with the flight N. 2 provide good results with a total error slightly higher than the best combination of two flights.

3.2. The Use of GCPs in the SfM-MVS processing

The required number of GCPs has been investigated using several combinations of GCPs selected from the 16 check points available. Therefore, we tested the planar and vertical accuracy of the 3D model generated using the survey N. 2 and the ensemble of images obtained from the

combination of flight N. 1 and 4. Approximately 64 combinations of GCPs, with a variable number ranging from 1 up to 9 (55% of the available check points), have been tested for each dataset providing useful guidelines on the appropriate strategy to improve the overall accuracy of resulting DSMs.

3.2.1. DSM derived from a single flight

In the present section, the accuracy assessment of the DSMs derived using the images from flight N.2 is described. This flight was selected among the many presented in the previous section, because it provided the best accuracy among the single flight options explored (see diagonal values of RMSE in Table 3).

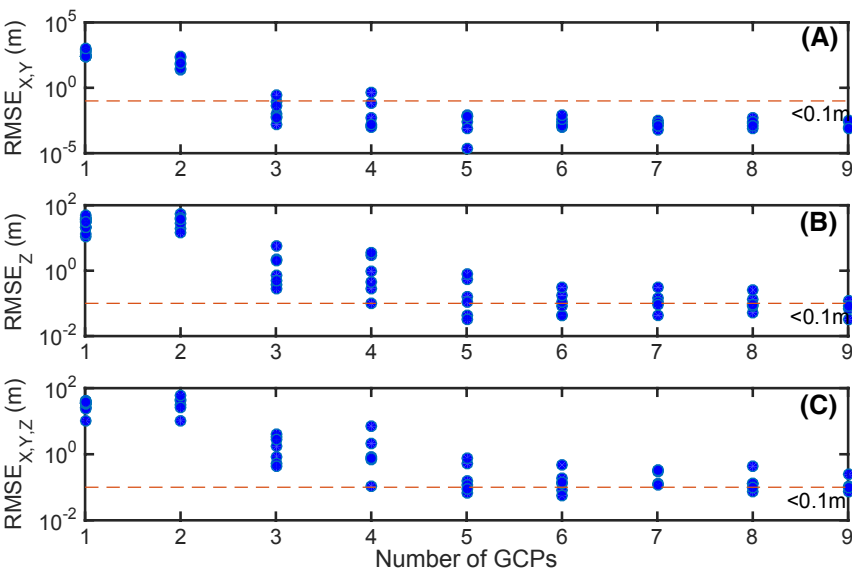


Figure 4. RMSE of the 3D model as a function of the number of GCPs adopted. A) RMSE in planar coordinates; B) RMSE in relative elevation; C) RMSE in X, Y, and Z obtained for the flight N.2.

Several DSMs have been generated using different combinations of GCPs modifying their number and relative distribution in space. Results of these analyses are summarized in Figure 4, where a sharp increase in DSM accuracy can be observed moving from 1 – 2 GCPs to 3 – 4 GCPs, with a mean error dropping from tens of meters to few meters only. This result is a well-known outcome due to the need of a minimum of three GCPs for the 3D transformation of coordinates.

The magnitude of planar errors is significantly reduced moving from four to five GCPs and seems to be fairly stable after five GCPs. On the other hand, vertical errors are always larger and tend to be more stable after six GCPs. In particular, planar error reaches values of few centimeters adopting only five GCPs (Figure 4), while vertical accuracy ranges from 6 – 74 cm for the same number of GCPs. Therefore the total error of DSM is influenced the most by higher values of RMSE_Z.

3.2.2. DSM derived from the combination of two flights

Adopting the combination of two flights the general patterns are similar to those observed in the previous section. Therefore, similar considerations can be made regarding the impact of GCPs numerosity. However, some key differences can be identified. Most notably, the RMSE's are generally lower when two flights of differing configurations are used, especially when more than six GCPs are adopted. In particular, the RMSE_{X,Y} is significantly below the threshold of 10 cm (the dashed line plotted in the graph), when more than 4 GCPs are adopted. RMSE_Z is less than 10 cm when more than six GCPs are adopted. Comparing the results of Figure 4 and 5, it can be noted that the errors in terms of planar coordinates (RMSE_{X,Y}) are comparable, but there is a critical difference in the elevation accuracy (RMSE_Z). This highlights the relative advantage of introducing two-flight combination in

the process, because the nadir orientation provides the best configuration for the planar coordinates, while the 20° tilted camera increases the vertical accuracy (see Table 3 for comparison).

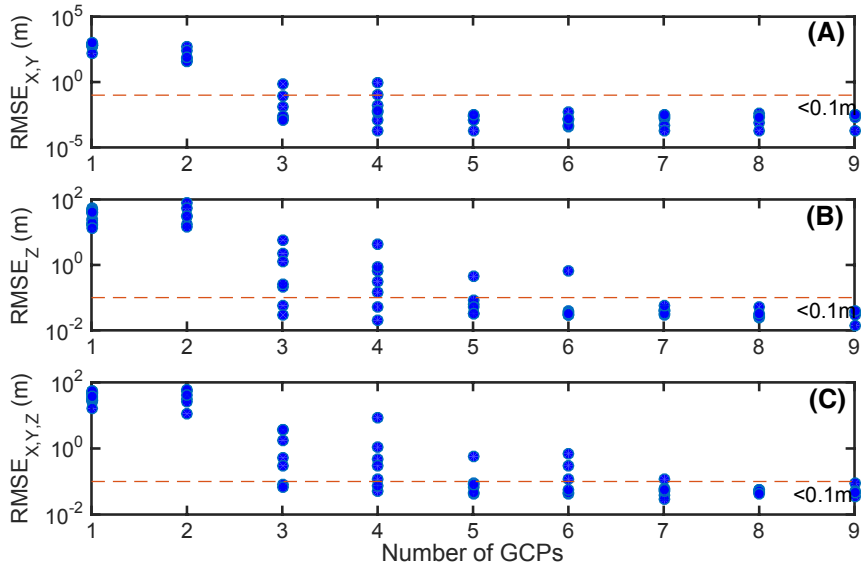


Figure 5. RMSE of the 3D model as a function of the number of GCPs adopted in the model run. A) RMSE in planar coordinates; B) RMSE in relative elevation; C) RMSE in X, Y, and Z for the combination of flights N.1 and N.4.

In order to emphasize the relative differences between the two configuration explored herein. Results obtained with a single flight and two flights are compared in Figure 6 that highlights the benefits of flight combination in terms of planar (panel A) and vertical (panel B) accuracy. The two configurations display minimal differences in terms of planar accuracy, while the results are significantly improved in the vertical precision when two flights are adopted. The DSMs obtained using a best combination of two flights reaches a vertical accuracy of about 3.5 cm if six or more GCPs are used. Moreover, the results seem to be relatively stable with more than six GCPs.

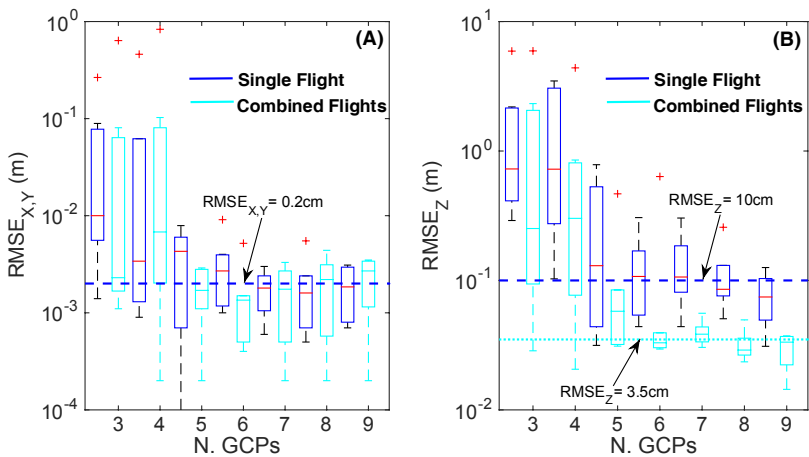


Figure 6. Comparison of results obtained changing the number of GCPs and adopting a single flight or a two flights dataset on the plane (A) and z-axes (B).

3.2.3. The spatial distribution of GCPs

The spatial distribution of GCPs controls strongly the DSM accuracy. Its influence has been explored looking at the relationship between the planar and vertical RMSE and the mean relative

distance between the GCPs on the plane (see Figure 7.A, C) and elevation (Figure 7.B, D). The analysis has been carried out for the two cases under investigation: 1) the single flight (Figure 7.A and B) and the combination of two flights (Figure 7.C and D). The RMSE associated with different number of GCPs are plotted using different colors to discriminate between the outputs obtained with different number of GCPs. It can be observed that each group is located in a portion of the graph (upper or lower) according to the number of GCPs. More GCPs the lower is generally their position on the graph. Nevertheless, all groups show a clear decrease of the errors with the increase of the mean distance both on the plane and on the z-axis.

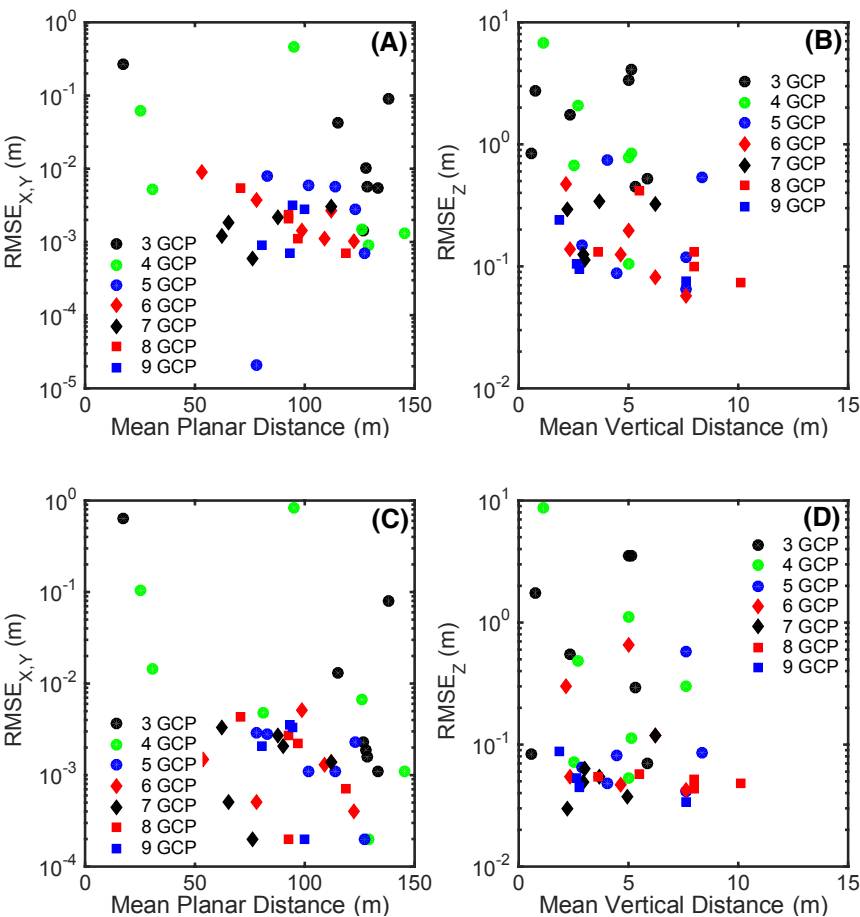


Figure 7. RMSE of the 3D model as a function of the mean distance between GCPs obtained for the flight N.2 (A, B) and for the combination of flights N.1 and N.4 (C, D).

4. Discussions

UAS-derived 3D models provide a new strategy to monitor land surface with an extremely high level of detail. The literature does not provide clear guidelines about operational use of UAS for 3D model reconstruction based on SfM-MVS algorithms, but several researchers explored different strategies aimed at minimizing the errors of 3D models. Review of these studies is extremely instructive to identify the control excerpted by the GCPs density on the planar and vertical accuracy of UAS-derived DSMs. Planar accuracy of SfM-MVS outputs are generally higher than vertical precision. This result impacts on the mean number of GCPs needed to improve the overall quality of the 3D model. In general, 5 GCPs/ha are enough to reach good performances on the plane, but 10 GCPs/ha are need to reach good precision in elevation (see Figure 1). Nevertheless, the final result is highly influenced by a number of factors such as flight pattern and configuration, camera quality, and local morphological complexity.

In our analysis, we focused on the 3D model optimization exploiting the combination of different flight configurations and the optimal GCPs design. For this reason, we explored the impact of : 1) the

combined use of images obtained from different flight patterns and configurations, and 2) the use of a variable number of GCPs. Both approaches are already used in practical application, still without clear identification of the benefits associated with combining images acquired using different flight plans and camera settings, nor the quantification of the impact of such choices. In addition, the density and distribution of GCPs remain open and not fully addressed.

According to our results it seems clear that the mission planning represents critical preliminary step that may significantly affect the final results. At certain circumstances, well-defined single flight may be sufficient to reach a fairly good quality of the overall survey. Nevertheless, the combination of flights with differing configurations can retrieve information from different viewpoints and angles that can certainly increase resulting accuracy. Given the optical nature of SfM-MVS algorithms, the challenge is to maximize the number of observations of each individual point retrieved across the area of interest. In this, the use of tilted camera may be beneficial in order to improve robustness of the geometrical model increasing the number of tie points describing inclined surfaces. Tilt of the camera should be defined according to both local morphology and resolution required. For the studied case characterized by trapezoidal earthen dam with an elevation of about 10 m and gentle slopes with elevation changes of 15 m, a tilt of 20° combined with a 0° flight were the best performing. This result can be justified by taking a closer look at the results reported on the diagonal of Table 3. In fact, the accuracy of planar coordinates is generally higher when using a nadir camera settings with lower flight altitude, but the vertical error is always lower for the flight with a 20° tilted camera. Therefore, the combination of the two flights tends to optimize both characteristics of DSMs.

The flights operated on two orthogonal routes provided additional benefits to the description of the area allowing a relevant reduction of error (for comparison see results of the combination 1 - 2). Comparing the accuracy of different DSMs obtained with a single flight or a combination of flights, the flight combination and tilted camera significantly increased the vertical accuracy, providing clear benefits to the process of DSM construction.

The error magnitude is also influenced by the flight altitude that controls image resolution. The use of multiple flights at different flight altitudes is a common practice to improve survey accuracy in aerophotogrammetry. We also observed a beneficial effect on the relative elevation accuracy of DSM, but such improvement is probably also influenced by the lower resolution of the images and in general is less effective than the use of a 20° tilted camera. Also in the literature, there are contrasting results on the relative impact of flight altitude, e.g. Gómez-Candón et al. [17] showed weak relationship of RMSE and flight height.

Orthorectification of orthomosaics is traditionally performed using GCPs, still other options should also be considered, such as investing in carrier phase GPS receiver and processing workflow that can help to reduce the amount of fieldwork needed in terms of GCP collection [24], especially useful if monitoring larger areas.

The new SfM-MVS algorithms have been markedly improving capabilities in construction of 3D models, but still the minimum number of GCPs needed to reach specific quality is uncertain. For example, Singh et al. [23] described weak negative relationship between GCPs and root mean square error (RMSE). Generally, at least three GCPs are necessary to allow the SfM-MVS algorithms to take advantage of such information. James et al. [10] recommend minimum of four to five GCPs, and emphasize accurate camera calibration, a factor not considered in our research. They showed that high RMSE for three GCPs decreases markedly for six GCPs especially for vertical component.

Our results show that with increasing number of GCPs there is an increase in quality of the 3D model that can reach values of few centimeters of planar RMSE (about 0.2cm) already for five GCPs. Vertical quality is generally lower, reaching centimeter precision (about 4cm) only if more than seven GCPs and two flights are adopted. This discrepancy of optimum number of GCPs recommended by different studies can partly be explained by the fact that for small number of GCPs, the error can be strongly influenced by their spatial distribution [10]. Indeed our results show that the spatial distribution of GCPs strongly controls the DSM accuracy, increasing with the mean GCP distance. This suggests that GCPs should be spread in space as much as possible to cover the entire range of variability in elevation and fulfil the extent of the area. These results corroborate the findings of James

and Robson [25] and Smith et al. [10] suggesting distribution of GCPs across and at the edges of the target area.

5. Conclusion

In the present manuscript, we tried to delineate some guidelines for UAS- surveys aimed at the derivation of 3D surface models. Exploiting the available literature on this topic and our field experiences, a number of indication can be derived:

- First of all the morphological complexity of the studied site represents the major difficulty for the surveys. The relevant changes observed in different study cases are mainly influenced by this factor. Nevertheless, accuracy can be improved increasing the number of GCPs, but elevation precision is the most challenging parameter.
- Flight pattern may significantly impact the result of the analysis. Therefore, it should be planned thoroughly to achieve the best vision of the entire area. Transversal survey with respect to a given structure provides a better description and quality of the resulting 3D surface.
- The use of images derived from different flights may be beneficial for DSM accuracy. In particular, the use of a tilted camera can improve the amount of information (retrieved number of points) for inclined surfaces providing higher DSM elevation accuracy. The presence of tilted camera images produces an increased robustness of the geometrical model providing a possible strategy to reduce the total number of GCPs adopted over a given area.
- The RMSE of the resulting 3D model reaches the value of few centimeters both in the plane and in vertical with minimal number of seven GCPs. This result must be considered site specific.
- Finally, we observed that the quality of the 3D model tends to increase when both relative plane and vertical distance of GCPs increases, suggesting potential strategy for their distribution in space. As a consequence, it is convenient to spread them in space as much as possible these points.

The experiment described herein cannot be considered exhaustive; still it provides insights into the problematic and can serve as a guideline for future applications. It is highly desirable to extend the analysis to new case studies and landscape morphologies in order to provide clear and more detailed guidelines for UAS applications. Nevertheless, the outcomes of the research lead to a number of useful contents that can support and guide UAS applications event in different morphological conditions. It is clear that there is not a unique response for the optimal number of GCPs that can optimize a survey, but our analysis helped understanding some general concepts. For instance, we should plan carefully our flights in order to optimize the amount of information retrieved by our cameras and also that the use of combined flight patterns can significantly improve the overall quality of the 3D models. That bears true even for the most critical dimension, which is the vertical one.

Author Contributions: S.M. conceived and coordinated the work and the writing; P.D., S.H., and J.J.A.J. supported the field activities and interpretation of the results; P.V. performed the numerical analysis; J.M. and M.P. supported the interpretation of the results and the writing.

Funding: This research was funded by the COST Action CA16219 “HARMONIOUS—Harmonization of UAS techniques for agricultural and natural ecosystems monitoring”. JM was supported by LTC18007 and RVO 67985939. PD was supported by LTC18007 and by the MEYS under the National Sustainability Programme I (Project LO1202).

Acknowledgments: In this section you can acknowledge any support given which is not covered by the author contribution or funding sections. This may include administrative and technical support, or donations in kind (e.g., materials used for experiments).

Conflicts of Interest: The authors declare no conflict of interest.

Appendix A: Dataset

In the present section, some of the most critical data derived from our analysis is reported in order to provide a full overview of the results and to give the possibility to readers to repeat some of the analysis reported herein. In the following, the tables with a list of the main characteristics of each SfM run are reported.

Number of GCP	RMSE _{x, y} (m)	RMSE _z (m)	RMSE _z (relative) (m)	Mean Planar distance (m)	Max Planar distance (m)	Mean Vertical distance (m)	Total distance (m)
2	184.070	55.100	40.920	8.45	8.45	2.17	10.61
2	57.540	18.580	30.630	40.34	40.34	0.09	40.43
2	24.7905	28.2890	10.2409	175.71	175.71	7.61	183.32
2	238.990	40.300	44.610	13.78	13.78	2.70	16.48
2	31.600	14.730	25.650	211.09	211.09	7.97	219.06
2	71.820	35.970	57.820	8.14	8.14	1.63	9.77
3	0.0892	2.1870	3.3477	138.22	207.32	5.03	143.25
3	0.265	5.910	4.070	17.39	26.05	5.11	22.50
3	0.010	0.726	1.735	127.78	191.33	2.36	130.14
3	0.0432	2.0284	2.7390	115.12	172.64	0.73	115.85
3	0.0058	0.3885	0.8351	128.19	191.44	0.57	128.76
3	0.0014	0.2904	0.5285	126.77	189.92	5.84	132.61
3	0.0055	0.4824	0.4484	133.18	177.09	5.30	138.48
4	0.0013	0.1028	0.1059	145.15	207.32	5.03	150.17
4	0.0053	0.9884	0.8459	30.78	49.51	5.11	35.89
4	0.0621	3.0553	2.0936	24.93	44.10	2.72	27.65
4	0.0009	0.2744	0.6726	129.22	226.61	2.55	131.77
4	0.03572	0.6726	0.6717	80.90	143.71	7.64	88.54
4	0.0015	0.4587	0.7903	125.73	207.32	5.03	130.76
4	0.4599	3.4737	6.8429	95.34	175.36	1.10	96.44
5	0.0058	0.7831	0.7491	113.61	209.12	4.05	117.66
5	0.00002	0.0315	0.0875	78.17	128.58	4.48	82.64
5	0.006	0.155	0.150	101.80	209.12	2.86	104.67
5	0.0028	0.1051	0.1182	123.03	226.61	7.61	130.64
5	0.0007	0.0439	0.0645	127.36	226.61	7.61	134.97
5	0.0079	0.5286	0.5332	83.05	143.71	8.32	91.38
6	0.0027	0.0442	0.0812	112.30	177.09	6.20	118.50
6	0.001	0.044	0.058	122.49	226.61	7.61	130.09
6	0.0014	0.0834	0.1949	98.83	207.32	5.03	103.85
6	0.0011	0.1074	0.1255	109.03	209.12	4.64	113.67
6	0.0038	0.1690	0.4740	77.91	177.09	2.18	80.09
6	0.0091	0.3059	0.1374	53.03	88.69	2.36	55.38
7	0.0020	0.0560	0.1200	90.08	209.12	4.94	95.02
7	0.003	0.044	0.327	112.30	177.09	6.20	118.50
7	0.0018	0.1455	0.2936	65.48	133.10	2.22	67.70
7	0.0022	0.1063	0.1257	87.51	211.09	2.92	90.43
7	0.0006	0.0934	0.1137	75.94	176.51	3.03	78.97
7	0.0012	0.3035	0.3379	62.35	93.08	3.65	66.00
8	0.0007	0.0506	0.0730	118.79	226.61	10.09	128.88
8	0.0021	0.1305	0.1316	92.43	226.61	3.62	96.05
8	0.0055	0.2573	0.4162	70.48	135.95	5.52	75.99
8	0.0024	0.0804	0.1318	92.79	211.09	7.97	100.76
8	0.0011	0.0905	0.0999	96.91	211.09	7.97	104.88
9	0.0028	0.0310	0.0747	99.71	226.61	7.61	107.32
9	0.0009	0.1258	0.2393	80.41	177.09	1.86	82.27
9	0.0031	0.0678	0.1045	94.67	211.09	2.64	97.30
9	0.0007	0.0812	0.0950	93.34	191.44	2.75	96.09

Table 4. Characteristics of the different SfM-MVS runs carried out with the dataset obtained from flight N.2.

Number of GCP	RMSE _{x,y} (m)	RMSE _z (m)	RMSE _z (relative) (m)	Mean Planar distance (m)	Max Planar distance (m)	Mean Vertical distance (m)	Total distance (m)
2	567.6526	76.9213	52.8201	8.45	8.45	2.17	10.61
2	54.4840	17.8242	30.8395	40.34	40.34	0.09	40.43
2	34.5736	30.2337	10.9425	175.71	175.71	7.61	183.32
2	275.0078	53.0793	57.9899	13.78	13.78	2.70	16.48
2	35.1901	15.1104	26.3944	211.09	211.09	7.97	219.06
2	70.2968	30.6586	42.1679	8.14	8.14	1.63	9.77
3	0.0806	2.3228	3.5662	138.22	207.32	5.03	143.25
3	0.6367	5.9248	3.5594	17.39	26.05	5.11	22.50
3	0.0019	0.2025	0.5453	127.78	191.33	2.36	130.14
3	0.0129	1.2650	1.7613	115.12	172.64	0.73	115.85
3	0.0016	0.0577	0.0826	128.19	191.44	0.57	128.76
3	0.0023	0.0286	0.0702	126.77	189.92	5.84	132.61
3	0.0011	0.2517	0.2947	133.18	177.09	5.30	138.48
4	0.0011	0.0206	0.0532	145.15	207.32	5.03	150.17
4	0.0146	0.1483	0.1143	30.78	49.51	5.11	35.89
4	0.1026	0.6844	0.4832	24.93	44.10	2.72	27.65
4	0.0002	0.0530	0.0726	129.22	226.61	2.55	131.77
4	0.0048	0.3018	0.3003	80.90	143.71	7.64	88.54
4	0.0068	0.8508	1.1049	125.73	207.32	5.03	130.76
4	0.8313	4.3809	8.6589	95.34	175.36	1.10	96.44
5	0.0011	0.0616	0.0644	101.80	209.12	2.86	104.67
5	0.0023	0.4664	0.5754	123.03	226.61	7.61	130.64
5	0.0002	0.0320	0.0413	127.36	226.61	7.61	134.97
5	0.0028	0.0845	0.0852	83.05	143.71	8.32	91.38
5	0.0011	0.0540	0.0485	113.61	209.12	4.05	117.66
5	0.0029	0.0311	0.0806	78.17	128.58	4.48	82.64
6	0.0014	0.0394	0.1176	112.30	177.09	6.20	118.50
6	0.0004	0.0295	0.0423	122.49	226.61	7.61	130.09
6	0.0052	0.6343	0.6602	98.83	207.32	5.03	103.85
6	0.0013	0.0345	0.0464	109.03	209.12	4.64	113.67
6	0.0005	0.0302	0.3019	77.91	177.09	2.18	80.09
6	0.0015	0.0315	0.0542	53.76	88.69	2.36	56.12
7	0.0021	0.0437	0.0370	90.08	209.12	4.94	95.02
7	0.0014	0.0394	0.1176	112.30	177.09	6.20	118.50
7	0.0005	0.0374	0.0300	65.48	133.10	2.22	67.70
7	0.0027	0.0304	0.0497	87.51	211.09	2.92	90.43
7	0.0002	0.0335	0.0627	75.94	176.51	3.03	78.97
7	0.0033	0.0558	0.0548	62.35	93.08	3.65	66.00
8	0.0007	0.0290	0.0483	118.79	226.61	10.09	128.88
8	0.0044	0.0235	0.0569	70.48	135.95	5.52	75.99
8	0.0027	0.0275	0.0513	92.79	211.09	7.97	100.76
8	0.0022	0.0312	0.0432	96.91	211.09	7.97	104.88
8	0.0002	0.0496	0.0542	92.43	226.61	3.62	96.05
9	0.0002	0.0144	0.0341	99.71	226.61	7.61	107.32
9	0.0021	0.0365	0.0883	80.41	177.09	1.86	82.27
9	0.0033	0.0302	0.0528	94.67	211.09	2.64	97.30
9	0.0035	0.0373	0.0444	93.34	191.44	2.75	96.09

Table 5. Characteristics of the different SfM-MVS runs carried out with the dataset obtained from flights N.1 – N.4.

The relative differences between the SfM-MVS runs with a single and two flights are summarized in Table 5. In particular, we report the mean value and the standard deviation of the RMSE obtained using the two datasets with differing numbers of GCPs. In this table, the advantage

in using a combination of flight configurations is obvious. It is mainly related to a significant reduction of the vertical error of the UAS-derived DSM.

Dataset from Flight N.2									
Number of GCPs/RMSE	1	2	3	4	5	6	7	8	9
Mean RMSE _{x,y} (m)	440.14	101.46	0.060	0.088	0.004	0.0032	0.0018	0.0024	0.0019
STD RMSE _{x,y} (m)	277.93	88.66	0.095	0.183	0.003	0.0031	0.0009	0.0019	0.0013
Mean RMSE _z (m)	30.25	32.16	1.716	1.392	0.274	0.1257	0.1385	0.1219	0.0764
STD RMSE _z (m)	10.89	14.90	2.008	1.486	0.309	0.0998	0.0991	0.0809	0.0392
Mean total RMSE (m)	33.44	34.97	1.957	1.892	0.283	0.1785	0.2396	0.1705	0.1284
STD total RMSE (m)	8.53	16.53	1.451	2.512	0.286	0.1524	0.1107	0.1395	0.075
Dataset from Flights N.1 and N. 4									
Mean RMSE _{x,y} (m)	680.65	172.87	0.105	0.137	0.002	0.0017	0.0017	0.002	0.0023
STD RMSE _{x,y} (m)	175.85	213.96	0.236	0.308	0.001	0.0018	0.0012	0.0017	0.0015
Mean RMSE _z (m)	33.81	37.30	1.436	0.920	0.122	0.1332	0.0400	0.0322	0.0296
STD RMSE _z (m)	14.24	23.60	2.151	1.559	0.170	0.2455	0.0090	0.0101	0.0106
Mean total RMSE (m)	37.62	36.86	1.411	1.541	0.149	0.2037	0.0586	0.0508	0.0549
STD total RMSE (m)	11.41	17.59	1.578	3.160	0.210	0.2444	0.0312	0.0053	0.0235

Table 6. The mean and standard deviation of the estimated RMSE depending on the number of GCPs.

References

1. Colomina, I.; Molina, P. Unmanned aerial systems for photogrammetry and remote sensing: A review. *ISPRS J. Photogramm. Remote Sens.* **2014**, *92*, 79–97, doi: 10.1016/j.isprsjprs.2014.02.013.

2. Whitehead, K.; Hugenholtz, C.H.; Myshak, S.; Brown, O.; LeClair, A.; Tamminga, A.; Barchyn, T.E.; Moorman, B.; Eaton, B. Remote sensing of the environment with small unmanned aircraft systems (UASs), part 2: Scientific and commercial applications. *J. Unmanned Veh. Syst.* **2014**, *2*, 86–102, doi:10.1139/juvs-2014-0006.

3. Manfreda, S.; McCabe, M.F.; Miller, P.; Lucas, R.; Pajuelo Madrigal, V.; Mallinis, G.; Ben Dor, E.; Helman, D.; Estes, L.; Ciruolo, G.; Müllerová, J.; Tauro, F.; De Lima, M.I.; De Lima, J.L.; Frances, F.; Caylor, K.; Kohv, M.; Maltese, A.; Perks, M.; Ruiz-Pérez, G.; Su, Z.; Vico, G.; Toth, B. On the Use of Unmanned Aerial Systems for Environmental Monitoring. *Remote Sens.* **2018**, *10*(4), 641; doi:10.3390/rs10040641.

4. Lucieer, A.; Jong, S. M. D.; & Turner, D. Mapping landslide displacements using Structure from Motion (SfM) and image correlation of multi-temporal UAV photography. *Progress in Physical Geography* **2014**, *38*(1), 97-116.

5. Clapuyt, F.; Vanacker, V.; Van Oost, K. Reproducibility of UAV-based earth topography reconstructions based on Structure-from-Motion algorithms. *Geomorphology* **2016**, *260*, 4-15, doi: 10.1016/j.geomorph.2015.05.011.

6. Cook, S.J.; Clarke, L.E.; Nield, J.M., *Geomorphological Techniques* (Online Edition). British Society for Geomorphology, London. ISSN: 2047-0371, **2012**.

7. Westoby, M. J.; Brasington, J.; Glasser, N. F.; Hambrey, M. J.; Reynolds, J. M. ‘Structure-from-Motion’ photogrammetry: A low-cost, effective tool for geoscience applications. *Geomorphology* **2012**, *179*, 300-314, doi: 10.1016/j.geomorph.2012.08.021.

8. Carrivick, J. L.; Smith, M. W. Quincey, D. J. *Structure from Motion in the Geosciences*. John Wiley & Sons, **2016**.

9. Smith, M.W.; Vericat, D. From experimental plots to experimental landscapes: topography, erosion and deposition in sub-humid badlands from structure-from-motion photogrammetry. *Earth Surf. Process. Landf.* **2015**, *40* (12), 1656–1671, doi: 10.1002/esp.3747.

10. James, M. R.; Robson, S.; d'Oleire-Oltmanns, S.; Niethammer, U. Optimising UAV topographic surveys processed with structure-from-motion: Ground control quality, quantity and bundle adjustment. *Geomorphology* **2017**, 280, 51-66, doi: 10.1016/j.geomorph.2016.11.021.
11. Ridolfi, E.; Buffi, G.; Venturi, S.; Manciola, P. Accuracy Analysis of a Dam Model from Drone Surveys. *Sensors* **2017**, 17, 1777, doi:10.3390/s17081777.
12. Rock, G.; Ries, J. B.; & Udelhoven, T. Sensitivity analysis of UAV-photogrammetry for creating digital elevation models (DEM). In Proceedings of Conference on Unmanned Aerial Vehicle in Geomatics **2011**.
13. Tahar, K. N. An evaluation on different number of ground control points in unmanned aerial vehicle photogrammetric block. *Int. Arch. Photogramm. Remote Sens. Spat. Inf. Sci* **2013**, 40, 93-98, doi: 10.3390/ecrs-2-05165.
14. Mancini, F.; Dubbini, M.; Gattelli, M.; Stecchi, F.; Fabbri, S.; Gabbianelli, G. Using unmanned aerial vehicles (UAV) for high-resolution reconstruction of topography: The structure from motion approach on coastal environments. *Remote Sensing* **2013**, 5(12), 6880-6898, doi:10.3390/rs5126880.
15. Hugenholtz, C.H.; Whitehead, K.; Brown O.W.; Barchyn, T.E.; Moorman, B.J.; LeClair, A.; Riddell, K., Hamilton, T. Geomorphological mapping with a small unmanned aircraft system (sUAS): Feature detection and accuracy assessment of a photogrammetrically-derived digital terrain model. *Geomorphology* **2013**, 194: 16-24. doi: 10.1016/j.geomorph.2013.03.023.
16. Cryderman, C.; Mah, S. B.; Shufletoski, A. Evaluation of UAV photogrammetric accuracy for mapping and earthworks computations. *Geomatica* **2014**, 68(4), 309-317, doi: 10.5623/cig2014-405.
17. Gómez-Candón, D.; De Castro, A. I.; López-Granados, F. Assessing the accuracy of mosaics from unmanned aerial vehicle (UAV) imagery for precision agriculture purposes in wheat. *Precision Agriculture* **2014**, 15(1), 44-56.
18. Uysal, M.; Toprak, A. S.; & Polat, N. DEM generation with UAV Photogrammetry and accuracy analysis in Sahitler hill. *Measurement* **2015**, 73, 539-543.
19. Küng, O.; Strecha, C.; Beyeler, A.; Zufferey, J. C.; Floreano, D.; Fua, P.; & Gervais, F. The accuracy of automatic photogrammetric techniques on ultra-light UAV imagery. In UAV-g 2011-Unmanned Aerial Vehicle in Geomatics **2011** (No. EPFL-CONF-168806).
20. Agüera-Vega, F.; Carvajal-Ramírez, F.; & Martínez-Carricondo, P. Assessment of photogrammetric mapping accuracy based on variation ground control points number using unmanned aerial vehicle. *Measurement* **2017**, 98, 221-227, doi: 10.1016/j.measurement.2016.12.002.
21. Koci, J.; Jarihani, B.; Leon, J. X.; Sidle, R. C.; Wilkinson, S. N.; & Bartley, R. Assessment of UAV and ground-based Structure from Motion with multi-view stereo photogrammetry in a gullied savanna catchment. *ISPRS International Journal of Geo-Information* **2017**, 6(11), 328.
22. Oniga, V.-E.; Breaban, A.-I.; Statescu, F. Determining the Optimum Number of Ground Control Points for Obtaining High Precision Results Based on UAS Images. *Proceedings* **2018**, 2, 352, doi: 10.3390/ecrs-2-05165.
23. Singh, K. K.; Frazier A.E. A meta-analysis and review of unmanned aircraft system (UAS) imagery for terrestrial applications, *Int. J. Remote Sens.* **2018**, doi: 10.1080/01431161.2017.1420941
24. Müllerová, J.; Bartaloš, T.; Brůna, J.; Dvořák, P.; & Vítková, M. Unmanned aircraft in nature conservation – an example from plant invasions. *Int. J. Remote Sens.* **2017**, 38 (8-10): 2177-2198; doi: 10.1080/01431161.2016.1275059
25. James, M.R.; Robson, S. Straightforward reconstruction of 3D surfaces and topography with a camera: Accuracy and geoscience application. *J. Geophys. Res. Earth Surf.* **2012**, 117, F03017.